Spin–orbit splitting of image states

2004 J. Phys.: Condens. Matter 16 6841

(http://iopscience.iop.org/0953-8984/16/39/017)

INSTITUTE OF PHYSICS PUBLISHING JOURNAL OF PHYSICS: CONDENSED MATTER

J. Phys.: Condens. Matter **16** (2004) 6841–6849 PII: S0953-8984(04)82617-1

Spin–orbit splitting of image states

J R McLaughlan, E M Llewellyn-Samuel and S Crampin[1]

Department of Physics, University of Bath, Bath, BA2 7AY, UK

E-mail: s.crampin@bath.ac.uk

Received 25 June 2004
Published 17 September 2004
Online at stacks.iop.org/JPhysCM/16/6841
doi:10.1088/0953-8984/16/39/017

Abstract

We quantify the effect of the spin–orbit interaction on the Rydberg-like series of image state electrons at the (111) and (001) surfaces of Ir, Pt and Au. Using relativistic multiple-scattering methods we find Rashba-like dispersions with $\Delta E^{\mathrm{SO}}(K) = \gamma K$ with values of γ for $n = 1$ states in the range 38–88 meV Å. Extending the phase accumulation model to include spin–orbit scattering we find that the splittings vary like $1/(n + a)^3$, where a is the quantum defect, and that they are related to the probability of spin-flip scattering at the surface. The splittings should be observable experimentally, being larger in magnitude than some exchange splittings that have been resolved by means of inverse photoemission, and are comparable to linewidths from inelastic lifetimes.

1. Introduction

Image states [1] are a special class of weakly bound surface electronic states in which an electron outside a dielectric or conductor polarizes the surface and is then attracted to the resulting 'image charge'. Asymptotically, the potential varies like $V(\boldsymbol{r}) \sim -1/z$, so a band gap preventing penetration of electrons into the crystal leads to a Rydberg-like series of states which in the case of a purely Coulombic image force at a planar metal surface arise at energies $E_n(\boldsymbol{K}) = -[0.85\ \mathrm{eV}]/n^2 + \hbar^2 K^2/2m$, $n = 1, 2, \ldots$ where $\boldsymbol{K}$ is the electron wavevector parallel to the surface and m the electron mass. Deviations from this behaviour reflect the influence and response of the surface-dependent electronic and atomic structure, which may therefore be investigated by studying image states. Examples of theoretical and experimental work include studies of the systematics of image state binding and dispersion on clean surfaces [2], image states on overlayers [3–5] and at stepped metal surfaces [6], exchange splitting of image states at ferromagnets [7–9], as well as image states at surface nanostructures [10–13]. In recent years there has also been considerable interest in the dynamics of image state electrons [14–17] as model electronic excitations at surfaces.

[1] Author to whom any correspondence should be addressed.

One aspect of the physics of image state electrons that has yet to be addressed is the influence of the spin–orbit interaction $H^{\mathrm{SO}} = (\hbar/4m^2c^2)\boldsymbol{\sigma}\cdot(\boldsymbol{\nabla}V_{\times}\boldsymbol{p})$ [18] which has recently been found to have a significant effect on other surface state electron levels at the surfaces of conductors with high atomic number [19, 20]. At first sight the spin–orbit interaction might be expected to be negligible. The mathematical analogy that can be drawn between the Schrödinger equation describing the electrons moving in the Coulomb-like image potential and that of s electrons in the hydrogen atom enables the image state wavefunctions to be written as

$$\psi_{n,\boldsymbol{K},s}(\boldsymbol{r}) = (1/8)zR_{n0}(z/4)\exp(\mathrm{i}\boldsymbol{K}\cdot\boldsymbol{r}_{\parallel})\chi_s \tag{1}$$

where $R_{n\ell}(r)$ is the normalized radial hydrogenic wavefunction and χ_s a Pauli spinor: $\chi_{\uparrow} = \binom{1}{0}$, $\chi_{\downarrow} = \binom{0}{1}$. Using these wavefunctions to diagonalize the spin–orbit perturbation H^{SO} in the subspace of degenerate image state levels gives a spin–orbit splitting of

$$\Delta E_n^{\mathrm{SO}} = \frac{\alpha^2 e^2 K}{64(4\pi\epsilon_0)n^3} = \left[0.012\ \mathrm{meV\ \AA}\right]\frac{K}{n^3} \tag{2}$$

where $\alpha = e^2/4\pi\epsilon_0\hbar c$ is the fine structure constant. This is well below the current resolution of inverse photoemission, two-photon photoemission and scanning tunnelling spectroscopy. However, it has previously been recognized that a more significant contribution to the spin–orbit splitting of 'crystal-derived' surface states arises from the brief time spent by the electron in the vicinity of the nuclei of the surface atoms, where the gradient contribution to the spin–orbit interaction is $|\boldsymbol{\nabla}V| \sim Z/r^2$. In this paper we report on calculations that we have performed to quantify the magnitude of the spin–orbit splitting that arises from the penetration of the image state wavefunction into the crystal at surfaces of Ir, Pt and Au. These are described in section 2. In section 3 we describe the modification of the phase accumulation model for image state energetics to include the effects of the spin–orbit interaction. Finally, we summarize and discuss our findings.

2. Relativistic electronic structure calculations

To calculate the spin–orbit splitting of image states we use a recently developed code that implements relativistic multiple-scattering theory. The theory behind this method is essentially that described by Halilov *et al* [21] so we do not reproduce it in detail here. The basic idea is that the electronic structure is found from the single-particle Green function corresponding to the Dirac Hamiltonian $\hat{H} = c\boldsymbol{\alpha}\cdot\boldsymbol{p} + \beta mc^2 + V$ [18]. Thus spin–orbit effects are treated non-perturbatively. Using scattering techniques the Green function is determined for the special case of semi-infinite crystals with two-dimensional in-plane translational periodicity, treating intralayer scattering within an angular momentum representation and interlayer scattering in a plane wave representation. Our calculations use 25 and 19 two-dimensional reciprocal lattice vectors to describe the interlayer scattering for the (001) and (111) surfaces respectively, and partial waves up to $\ell_{\max} = 4$ [22]. The semi-infinite substrate means that continuum and surface-localized states are clearly distinguished in the wavevector resolved local density of states, found from the imaginary part of the Green function. As in the non-relativistic version of the code [23], the electronic structure is found self-consistently using the local density approximation to density functional theory. We use the atomic sphere approximation for the crystal potential (including dipole contributions), with the potential in the three outermost atomic layers allowed to vary in response to the presence of the surface. Since the local density approximation does not lead to an image-like surface barrier, and hence does not support image states, once self-consistency has been achieved we replace the self-consistent barrier with a

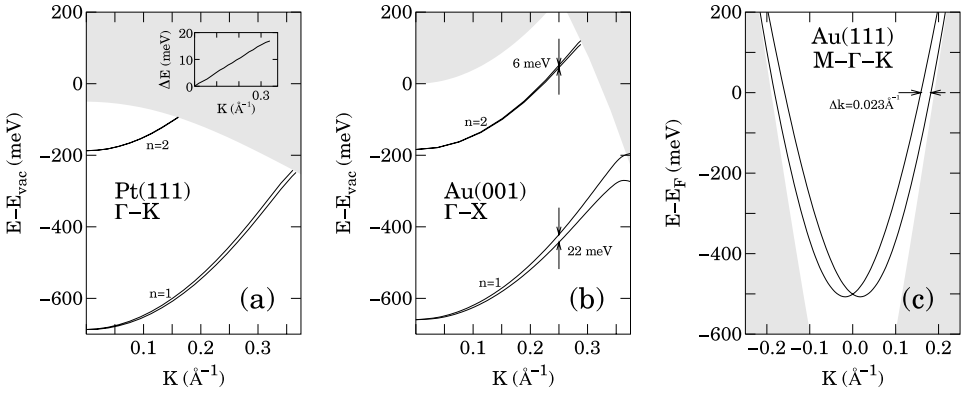

Figure 1. Calculated surface state dispersion curves. The shading indicates the presence of bulk or vacuum continuum states. (a) Pt(111) $n = 1$ and 2 image states. The inset demonstrates that the splitting of the $n = 1$ state is linear in K. (b) Au(001) $n = 1$ and 2 image states. (c) The Au(111) surface state (note that the energy scale in this case is with reference to the Fermi level).

parametrized model barrier, for which we use the 'JJJ' potential [24]

$$V_{\mathrm{B}}(z) = \begin{cases} \left(1 - \mathrm{e}^{\lambda(z-z_0)}\right)/4(z - z_0), & z < z_0, \\ -U/\left(1 + A\mathrm{e}^{-\beta(z-z_0)}\right), & z > z_0. \end{cases} \tag{3}$$

The fitting parameters λ, U and z_0 were fixed by starting with values quoted by Smith *et al* [25], who fitted to first-principles slab calculations, and then adjusted slightly to place the $n = 1$ image state at $K = 0$, E_1, close to values found experimentally. The procedure does not uniquely fix the parameters, but we found that different combinations that gave the same value for E_1 resulted in almost identical image state dispersion curves. Note that our results are for the 1×1 unreconstructed surfaces of the materials studied. In several cases the surfaces undergo complex surface reconstructions (e.g. Au(001) and Pt(001) adopt a 5×20 reconstruction but may be prepared in the 1×1 structure—see [26]).

In figure 1 we illustrate the dispersion curves that we find. For both Pt(111) and Au(001) the spin–orbit interaction can clearly be seen to split the $n = 1$ image state, and whilst a splitting exists for the $n = 2$ and higher states it is much smaller. The inset in the figure 1(a) illustrates the variation of the splitting with wavevector K, the near-linear variation corresponding to a Rashba-like dispersion [27, 28]

$$E_n(K) \simeq E_n + \frac{\hbar^2 K^2}{2m} \pm (\gamma/2)K. \tag{4}$$

From curves such as these we extract Rashba parameters γ by a least-squares fit using wavevectors $K \leqslant 0.2$ Å^{-1}. These values are tabulated in table 1 for the image states at the (111) and (001) surfaces of Ir, Pt and Au. At Au(111) the vacuum level lies outside of the projected band gap, so the image states in this case exist as resonances. We have not therefore included results for this case, but instead give the results that we find for the spin–orbit splitting of the occupied surface state that occurs within the band gap at this surface. The dispersion of this state is shown also in figure 1, and agrees well with previous work, validating our procedure. We find that the wavevector splitting at the Fermi energy is $\Delta k = 0.023$ Å^{-1}, compared with experimental values of 0.023 Å^{-1} [19], 0.025 Å^{-1} [31, 32] and 0.027 Å^{-1} [36], and a theoretical value of 0.023 Å^{-1} [37], that have been reported previously.

The results in table 1 indicate that the spin–orbit splitting of $n = 1$ image states at Ir, Pt and Au surfaces is an order of magnitude smaller than that of the Au(111) Shockley surface state,

Table 1. Calculated image state energies including the spin–orbit interaction at (001)-1 × 1 and (111)-1 × 1 surfaces of Ir, Pt and Au: $E_n(K) = E_n + \hbar^2K^2/2m \pm (\gamma/2)K$. E_n values in brackets are from experiment.

Surface	n	E_n (eV)	$m(m_e)$	γ (meV Å)
Ir(111)	1	−0.65	0.95	56 ± 1
	2	−0.18	1.00	9 ± 1
Ir(001)	1	−0.61	0.94	38 ± 1
	2	−0.17	0.99	6 ± 1
Pt(111)	1	−0.69 (−0.65[a], −0.78[b])	1.05	50 ± 2
	2	−0.19 (−0.16[a], −0.20[b])	1.03	8 ± 1
Pt(001)	1	−0.60 (−0.60[c])	0.96	47 ± 2
	2	−0.17	0.99	9 ± 1
Au(111)	SS	−0.50 (−0.41[d], −0.49[e] − 0.51[f])	0.23	800 ± 50
Au(001)	1	−0.66 (−0.69[g], −0.63[h])	1.05	88 ± 4
	2	−0.18	1.05	20 ± 2

[a] See [29].
[b] See [30].
[c] See [26].
[d] See [19].
[e] See [31].
[f] See [33].
[g] See [34].
[h] See [35].

and that of the $n = 2$ states smaller still. These trends reflect the differing extents to which the corresponding wavefunctions penetrate the crystal and experience the spin–orbit interaction at the ion cores. At the (001) surfaces $\Delta E_n^{\mathrm{Ir}} < \Delta E_n^{\mathrm{Pt}} < \Delta E_n^{\mathrm{Au}}$, which might be expected given the increasing atomic number ($Z^{\mathrm{Ir}} = 77$, $Z^{\mathrm{Pt}} = 78$, $Z^{\mathrm{Au}} = 79$), but at the (111) surface $\Delta E_n^{\mathrm{Ir}} > \Delta E_n^{\mathrm{Pt}}$, pointing to a more complicated 'band-structure' effect. In figure 1 the splitting of the Au(001) $n = 1$ image state is also seen to be affected as it disperses towards the band edge of continuum levels. We return to this later.

3. Phase accumulation model

The 'standard model' for understanding image state energies is the phase accumulation model [1] in which surface states are envisaged as one-dimensional waves trapped by multiple reflection from the surface barrier and the crystal. In a region of constant potential (see figure 2) between the barrier and crystal (which may be infinitesimal in width), the electron wavefunction can be expressed in terms of forward and backward travelling plane waves:

$$\psi(z) = A\exp(\mathrm{i}kz) + B\exp(-\mathrm{i}kz). \tag{5}$$

The two components are related at the barrier reference plane $z = z_{\mathrm{B}}$ by the barrier reflection coefficient r_{B}, $\psi(z) \propto \exp(-\mathrm{i}k(z - z_{\mathrm{B}})) + r_{\mathrm{B}}\exp(\mathrm{i}k(z - z_{\mathrm{B}}))$ and at the crystal reference plane $z = z_{\mathrm{C}}$ by the crystal reflection coefficient r_{C}, $\psi(z) \propto \exp(\mathrm{i}k(z - z_{\mathrm{C}})) + r_{\mathrm{C}}\exp(-\mathrm{i}k(z - z_{\mathrm{C}}))$, which together with (5) give rise to the condition for a surface state to exist:

$$r_{\mathrm{B}}r_{\mathrm{C}}\exp(2\mathrm{i}kd) - 1 = 0, \qquad d = z_{\mathrm{B}} - z_{\mathrm{C}}. \tag{6}$$

For energies below the vacuum level and coincident with the crystal band gap the reflection probabilities at both crystal and barrier are unity and the reflection coefficients may be written in terms of phases: $r_{\mathrm{B}} = \exp(\mathrm{i}\phi_{\mathrm{B}})$, $r_{\mathrm{C}} = \exp(\mathrm{i}\phi_{\mathrm{C}})$. The surface state condition then becomes

$$\phi_{\mathrm{B}} + \phi_{\mathrm{C}} + 2kd = 2\pi n, \qquad n = 0, 1, \ldots, \tag{7}$$

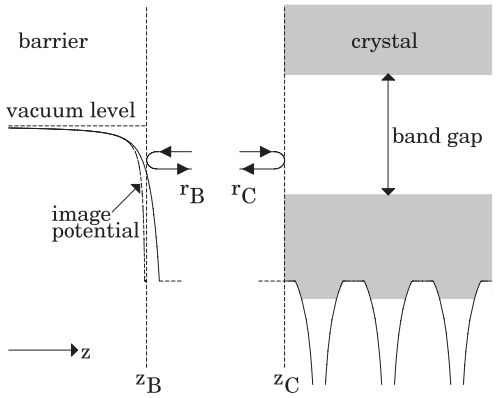

Figure 2. A schematic illustration of quantities entering the phase accumulation model.

which is a condition on the round-trip phase accumulated by the electron wave. The phases in (7) increase with energy. The crystal phase increases from 0 to π as the energy sweeps across the band gap, changing most rapidly near the band edges. Towards the bottom of the gap it is this variation in ϕ_C which will determine whether or not (7) is satisfied, so any surface state that does arise is usually referred to as 'crystal derived'. On the other hand, ϕ_B increases more and more rapidly as the energy approaches the vacuum energy, varying to a good approximation as

$$\phi_B(E) = \pi\left(\sqrt{\frac{3.4\ \mathrm{eV}}{-E}} - 1\right). \tag{8}$$

In combination with (7) this yields a Rydberg-like series of image states

$$E_n = \frac{-0.85\ \mathrm{eV}}{(n+a)^2}, \qquad n = 1, 2, \ldots, \tag{9}$$

where the quantum defect $a = (1 - [\phi_C + 2kd]/\pi)/2$ may usually be considered constant over the range of energies at which the image states are found.

We now consider the extension of this model to include the spin–orbit interaction. Introducing the electron spin in the wavefunction in (5):

$$\psi(z) = \begin{pmatrix}\psi_\uparrow(z)\\ \psi_\downarrow(z)\end{pmatrix} = \begin{pmatrix}A_\uparrow\\ A_\downarrow\end{pmatrix}\exp(\mathrm{i}kz) + \begin{pmatrix}B_\uparrow\\ B_\downarrow\end{pmatrix}\exp(-\mathrm{i}kz), \tag{10}$$

and reflection from the crystal is now described by a matrix:

$$R_C = \begin{pmatrix} r_C^{\uparrow\uparrow} & r_C^{\uparrow\downarrow}\\ r_C^{\downarrow\uparrow} & r_C^{\downarrow\downarrow}\end{pmatrix} \tag{11}$$

allowing for the possibility of spin-flip upon reflection. With a similar matrix used to describe scattering from the barrier, the condition for a surface state becomes

$$\det\left[R_B R_C \exp(2\mathrm{i}kd) - 1\right] = 0. \tag{12}$$

The four reflection coefficients in (11) are not independent—for example flux conservation requires that $|r_C^{\uparrow\uparrow}|^2 + |r_C^{\downarrow\uparrow}|^2 = 1$ within a gap, and for a non-magnetic crystal $r_C^{\uparrow\uparrow} = r_C^{\downarrow\downarrow}$. In the non-magnetic case and for a planar potential $V = V(z)$ the electron wavefunctions $\Psi_{\boldsymbol{K}}(\boldsymbol{r}) = \psi_{\boldsymbol{K}}(z)\exp(\mathrm{i}\boldsymbol{K}\cdot\boldsymbol{r}_\parallel)$ are found from the Hamiltonian

$$H = -\frac{\hbar^2}{2m}\nabla^2 + V + \frac{\hbar^2}{4m^2c^2}\boldsymbol{\sigma}\cdot(\boldsymbol{\nabla}V_\times\boldsymbol{K}). \tag{13}$$

which may be diagonalized by a rotation in spin space:

$$H' = U_\vartheta H U_\vartheta^{-1} = -\frac{\hbar^2}{2m}\nabla^2 + V + \frac{\hbar^2 K}{4m^2c^2}\frac{\mathrm{d}V}{\mathrm{d}z}\sigma_z \tag{14}$$

with

$$U_\vartheta = \frac{1}{\sqrt{2}}\begin{pmatrix} 1 & -\mathrm{i}\exp(-\mathrm{i}\vartheta) \\ 1 & +\mathrm{i}\exp(-\mathrm{i}\vartheta) \end{pmatrix} \tag{15}$$

where ϑ is the angle of the electron wavevector. The Hamiltonian H' does not mix spin-up and spin-down channels and so in this representation the reflection matrix describing scattering from the crystal is diagonal:

$$R'_\mathrm{C} = \begin{pmatrix} r_\mathrm{C}^+ & 0 \\ 0 & r_\mathrm{C}^- \end{pmatrix}. \tag{16}$$

Since the spin–orbit interaction is negligible in the barrier, the barrier reflection matrix is also diagonal and, for a non-magnetic surface, $R_\mathrm{B}^{\uparrow\uparrow} = R_\mathrm{B}^{\downarrow\downarrow} = r_\mathrm{B}^+ = r_\mathrm{B}^- = r_\mathrm{B}$, so the surface state condition (12) becomes $r_\mathrm{C}^\pm r_\mathrm{B}\exp(2\mathrm{i}kd) = 1$ leading to the round-trip phase condition

$$\phi_\mathrm{C} \pm \eta + \phi_\mathrm{B} + 2kd = 2\pi n, \qquad n = 1, 2, \ldots, \tag{17}$$

where we have introduced $r_\mathrm{C}^\pm = \exp(\mathrm{i}(\phi_\mathrm{C} \pm \eta))$ appropriate to energies within a gap. The surface states now come in spin split pairs, with spin orientations that may be deduced from the spinors that are obtained by rotating back into the original reference frame the spin-up and spin-down eigenspinors $\chi'^{+} = \binom{1}{0}$, $\chi'^{-} = \binom{0}{1}$ of the primed frame:

$$\chi_\vartheta^\pm = U_\vartheta^{-1}\chi'^{\pm} = \frac{1}{\sqrt{2}}\begin{pmatrix} 1 \\ \pm\mathrm{i}\exp(\mathrm{i}\vartheta) \end{pmatrix}. \tag{18}$$

Thus $\widehat{\boldsymbol{S}} = \pm(-\sin\vartheta, \cos\vartheta, 0) = \pm\widehat{z}\times\widehat{K}$ and we find that the spins lie in the surface plane and perpendicular to $\boldsymbol{K}$, to the left (right) for + (−).

Rotating back to the original spin frame gives the reflection matrix (11) as

$$R_\mathrm{C} = U_\vartheta^{-1} R'_\mathrm{C} U_\vartheta = \exp(\mathrm{i}\phi_\mathrm{C})\begin{pmatrix} \cos\eta & \exp(-\mathrm{i}\vartheta)\sin\eta \\ -\exp(\mathrm{i}\vartheta)\sin\eta & \cos\eta \end{pmatrix}. \tag{19}$$

In figure 3 we illustrate the variation in $\tan\eta$ at the Au(001) surface calculated from the reflection matrix found using the relativistic multiple-scattering method of section 2. For $\boldsymbol{K}$ along $\overline{\Gamma}\,\overline{\mathrm{X}}$ (see the inset in figure 3), equation (19) gives $\tan\eta = r^{\uparrow\downarrow}/r^{\uparrow\uparrow}$. The relativistic multiple-scattering calculations include the atomic structure of the surface and the crystal potential is not one-dimensional, but the reflection coefficient for specular reflection behaves in a very similar manner to that of a one-dimensional crystal, especially for small K where the wavefunction varies only slowly across the surface. In particular, we find that the angular variation predicted by equation (19) is satisfied to within one per cent or so. It is evident from figure 3 that the magnitude of the spin–orbit induced phase change is small, and away from the band edges η is approximately independent of energy at Au(001) and linear in K: $\eta_{(001)}^{\mathrm{Au}}(E, K) \simeq [-0.25\ \text{Å}]K$.

To first order, the round-trip phase condition (17) is satisfied at energies $E_n \pm \Delta E_n^{\mathrm{SO}}/2$ where

$$\Delta E_n^{\mathrm{SO}} \simeq -2\eta\left(\frac{\mathrm{d}}{\mathrm{d}E}(\phi_\mathrm{B} + \phi_\mathrm{C} + 2kd)\bigg|_{E_n}\right)^{-1}, \tag{20}$$

neglecting the energy dependence of η which is small compared to those for the other phases. For all the surfaces that we have studied we have found that η does not change sign across

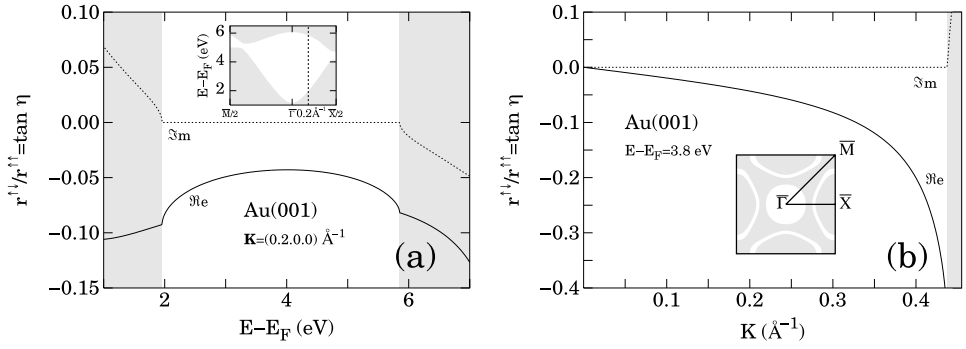

Figure 3. The variation of the spin-flip to non-spin-flip scattering ratio $r^{\uparrow\downarrow}/r^{\uparrow\uparrow}$ for Au(001) in the major band gap of the projected band structure. (a) As a function of energy at $\boldsymbol{K} = (0.2, 0.0)$ Å^{-1}. (b) As a function of wavevector along $\overline{\Gamma}\,\overline{\mathrm{X}}$ at the mid-gap energy. The inset shows the projected gaps across the Brillouin zone at the same energy.

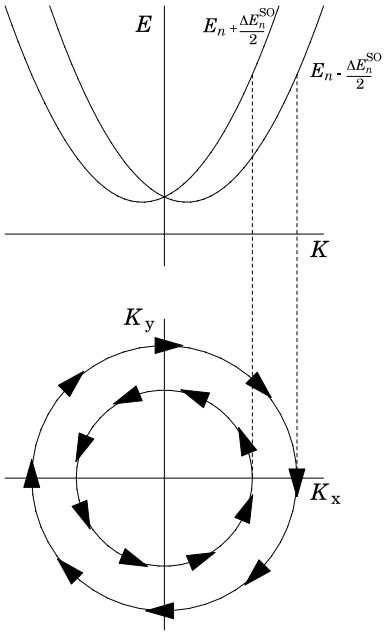

Figure 4. Spin orientation of spin–orbit split surface states for $\eta < 0$.

the band gap, and the denominator in (20) is positive. Hence the model predicts a series of spin–orbit split states with identical spin orderings, which we have confirmed is also the case in the relativistic multiple-scattering calculations described in section 2. In particular with $\eta < 0$ the surface states that exist are split with the lower of each pair of levels having the spin pointing to the right of $\boldsymbol{K}$, as shown in figure 4. This is in agreement with the spin assignments shown in Henk *et al* [37] for the Au(111) surface state, but disagrees with those given in [31].

When the gap contains image states, over the narrow range of energies within which the image states are found, the energy dependence of the round-trip phase is dominated by the

variation in the barrier phase (8) and then

$$\Delta E_n^{\mathrm{SO}} \simeq -2\eta \left(\left. \frac{\mathrm{d}\phi_{\mathrm{B}}}{\mathrm{d}E} \right|_{E_n} \right)^{-1} = -\frac{\eta \times 1.7\ \mathrm{eV}}{\pi (n+a)^3}. \tag{21}$$

Thus the spin splittings exhibit the same scaling as the lifetime broadening [1], in each case the behaviour ultimately originating in the variation with n of the wavefunction overlap with the crystal. We also see from (21) that the linear-in-K behaviour of ΔE_n^{SO} arises from similar behaviour of η. Since η is small, $\tan\eta \simeq \sin\eta \simeq \eta$ to a good approximation, and hence $\eta \simeq -|r^{\uparrow\downarrow}|$. Thus the spin–orbit splitting is directly related to the spin-flip scattering rate, which could therefore be determined from experimental values of image state splittings. At Au(001), $E_1 \simeq -0.66$ meV (table 1), so combining equations (9) and (21) gives

$$\Delta E_1^{\mathrm{SO}} \simeq -\eta \times \frac{1.7\ \mathrm{eV}}{\pi} \left(\frac{0.66}{0.85} \right)^{3/2} = -\eta \times 0.37\ \mathrm{eV} \tag{22}$$

and a splitting of 22 meV (figure 1) at $K = 0.25$ Å^{-1} yields $\eta \simeq 0.06$, which agrees with the value found from the multiple-scattering calculations shown in figure 3. Finally, we note that equation (21) will not hold near band edges where the energy dependence of the crystal phase ϕ_{C} cannot be neglected. This is the origin of the anomalous dispersion shown for the $n = 1$ state at Au(001) in figure 1.

4. Discussion

To summarize, we have investigated the effect of the spin–orbit interaction on image state electrons at the (111) and (001) surfaces of Ir, Pt and Au. Non-perturbative calculations that use relativistic multiple-scattering theory with self-consistent potentials and a parametrized surface barrier predict Rashba-like dispersion of the image state bands with splittings for $n = 1$ that are a factor 10–20 times smaller than that of the Au(111) Shockley state, for which our results are in good agreement with experiment and previous theory. Extending the phase accumulation model to include spin–orbit scattering, we find that the splittings scale as $1/(n + a)^3$, where a is the quantum defect, and are directly related to the spin-flip scattering rate at the surface. The largest image state splittings that we find are at Au(001) for which $\Delta E_1^{\mathrm{SO}} = 22$ meV at $K = 0.25$ Å^{-1}. This is larger than some exchange splittings of image states that have previously been resolved (e.g. 18 ± 13 meV at Ni(111) [7] and 13 ± 13 meV at Ni(001) [38]) by exploiting the spin resolution available in spin-resolved inverse photoemission, suggesting that the spin–orbit splitting may also be observable with an appropriate experimental set-up. The splittings are comparable to lifetime broadenings of late transition and noble metal image states [14, 16], indicating that accounting for spin–orbit effects may be necessary when determining image state lifetimes from lineshape analysis for 5d metals.

References

[1] Echenique P M and Pendry J B 1978 *J. Phys. C: Solid State Phys.* **11** 2065
[2] Straub D and Himpsel F J 1986 *Phys. Rev.* B **33** 2256
[3] Padowitz D F, Merry W R, Jordan R E and Harris C B 1992 *Phys. Rev. Lett.* **69** 3583
[4] Fischer R, Schuppler S, Fisher N, Fauster Th and Steinmann W 1993 *Phys. Rev. Lett.* **70** 654
[5] Wallauer W and Fauster Th 1996 *Phys. Rev.* B **54** 5096
[6] Smadici S, Mocuta D and Osgood R M 2004 *Phys. Rev.* B **69** 035415
[7] Passak F and Donath M 1992 *Phys. Rev. Lett.* **69** 1101

[8] Nekovee M, Crampin S and Inglesfield J E 1993 *Phys. Rev. Lett.* **70** 3099
[9] De Rossi S, Ciccacci F and Crampin S 1996 *Phys. Rev. Lett.* **77** 908
[10] Fischer R, Fauster Th and Steinmann W 1993 *Phys. Rev.* B **48** 15496
[11] Ortega J E, Himpsel J F, Haight R and Peale D R 1994 *Phys. Rev.* B **49** 13859
[12] Hill I G and McLean A B 1999 *Phys. Rev. Lett.* **82** 2155
[13] Kasperovich V, Wong K, Tikhonov G and Kresin V V 2000 *Phys. Rev. Lett.* **85** 2729
[14] Echenique P M, Pitarke J M, Chulkov E V and Rubio A 2000 *Chem. Phys.* **251** 1
[15] Wahl P, Schneider M A, Diekhöner L, Vogelgesang R and Kern K 2003 *Phys. Rev. Lett.* **91** 106802
[16] Rhie H-S, Link S, Dürr H A, Eberhardt W and Smith N V 2003 *Phys. Rev.* B **68** 033410
[17] Boger K, Weinelt M and Fauster Th 2004 *Phys. Rev. Lett.* **92** 126803
[18] Messiah A 1962 *Quantum Mechanics* vol 2 (Amsterdam: North-Holland)
[19] LaShell S, McDougall B A and Jensen E 1996 *Phys. Rev. Lett.* **77** 3419
[20] Rotenberg E, Chung J W and Kevan S D 1999 *Phys. Rev. Lett.* **82** 4066
[21] Halilov S V, Tamura E, Meinert D, Gollisch H and Feder R 1993 *J. Phys.: Condens. Matter* **5** 3859
[22] Crampin S 1994 *Phys. Rev.* B **49** 14035
[23] Crampin S 1993 *J. Phys.: Condens. Matter* **5** 4647
[24] Jones R O, Jennings P J and Jepsen O 1984 *Phys. Rev.* B **29** 6474
[25] Smith N V, Chen C T and Weinert M 1989 *Phys. Rev.* B **40** 7565
[26] Drube R, Dose V and Goldmann A 1988 *Surf. Sci.* **197** 317
[27] Rashba E I 1960 *Sov. Phys.—Solid State* **2** 1109
[28] Bychkov Y A and Rashba E I 1984 *JETP Lett.* **39** 78
[29] Link S, Dürr H A, Bihlmayer G, Blügel S, Eberhardt W, Chulkov E V, Silkin V M and Echenique P M 2001 *Phys. Rev.* B **63** 115420
[30] Kinoshita I, Anazawa T and Matsumoto Y 1996 *Chem. Phys. Lett.* **259** 445
[31] Nicolay G, Reinert F, Hüfner S and Blaha P 2001 *Phys. Rev.* B **65** 033407
[32] Reinert F 2003 *J. Phys.: Condens. Matter* **15** S693
[33] Kliewer J, Berndt R, Chulkov E V, Silkin V M, Echenique P M and Crampin S 2000 *Science* **288** 1399
[34] Ciccacci F, De Rossi S, Taglia A and Crampin S 1994 *J. Phys.: Condens. Matter* **6** 7227
[35] Straub A and Himpsel F J 1984 *Phys. Rev. Lett.* **52** 1922
[36] Mugarza A *et al* 2002 *Phys. Rev.* B **66** 245419
[37] Henk J, Ernst A and Bruno P 2003 *Phys. Rev.* B **68** 165416
[38] Starke K, Ertl K and Dose V 1992 *Phys. Rev.* B **45** 6154